nature materials

LETTERS

PUBLISHED ONLINE: 13 JANUARY 2013 | DOI: 10.1038/NMAT3496

# Entropy favours open colloidal lattices

Xiaoming Mao[1,2]*, Qian Chen[3] and Steve Granick[3,4,5]

**Burgeoning experimental and simulation activity seeks to understand the existence of self-assembled colloidal structures that are not close-packed[1–9]. Here we describe an analytical theory based on lattice dynamics and supported by experiments that reveals the fundamental role entropy can play in stabilizing open lattices. The entropy we consider is associated with the rotational and vibrational modes unique to colloids interacting through extended attractive patches[10]. The theory makes predictions of the implied temperature, pressure and patch-size dependence of the phase diagram of open and close-packed structures. More generally, it provides guidance for the conditions at which targeted patchy colloidal assemblies in two and three dimensions are stable, thus overcoming the difficulty in exploring by experiment or simulation the full range of conceivable parameters.**

There is intense interest in creating open crystalline arrangements of spheres, arrangements less dense than close-packed, as they have predicted applications in photonics, catalysis, and porous media[11,12] and also an interesting response to mechanical stress[13–18]. A general instability argument due to Maxwell[13] explains the challenge: periodic lattices formed by particles connected by central force bonds, most homogeneous colloids for example, possess mechanical stability only if their mean coordination number $z$ exceeds the 'isostatic' value of $2d$, where $d$ is the spatial dimension[13]. Here, one central force bond acts as one constraint against zero energy distortions. For a finite piece of isostatic lattice, owing to the deficit of constraints on the boundary, the number of floppy modes is subextensive, and to achieve mechanical stability the lattice needs additional constraints. Depending on the architecture of the lattice, under periodic boundary conditions these floppy modes can either remain at zero energy or be lifted to finite energy. For details see ref. 17. Most open lattices are unstable by this criterion. For example, the absence of a potential energy penalty for bond-angle changes allows 'floppy modes' in an open kagome lattice; these zero-energy lattice distortions collapse the lattice into a close-packed hexagonal lattice[17], as we illustrate in Fig. 1a.

Theorists have proposed a variety of additional constraints to lift the energy of floppy modes, principally attractive 'glue' points or interactions beyond nearest neighbours[1–4], but it has been challenging to implement these ideas in the laboratory. Our puzzle here is to explain recent laboratory observations of a stable open lattice whose origin seems to be different[5]. Performed in colloidal monolayers such that $d = 2$, the spheres lack specific glue points or other complex potentials that had been proposed theoretically[1–4]. Their mutual attraction of a simple short-range nature is restricted to attractive areas at the north and south poles of the sphere, large enough to allow a family of bond-angle changes without increase of the potential energy ('triblock Janus spheres')[5]. The conventional theoretical analysis predicts the multiple isoenergetic structures depicted in Fig. 1b,c, but in the laboratory solely the kagome lattice structure was observed. This is because conventional theory on open lattices just counts energetic constraints, whereas colloidal assemblies can be strongly affected by thermal fluctuations. Entropic effects have been studied for homogeneous colloidal particles[19,20]; in this communication we investigate the subtle differences that are unique to patchy colloids yet crucial to phase selection of stable open lattices.

To describe the restricted rotations of patchy particles in a lattice, we modify the formalism of lattice dynamics for atomic systems, starting from the generic form of partition function of the lattice applicable to any patchy particle system,

$$Z = \int \mathrm{e}^{-H(\{\mathbf{r}_i,\theta_i\})/k_\mathrm{B}T} \prod_j \mathrm{d}\mathbf{r}_j \, \mathrm{d}\theta_j \qquad (1)$$

where $H$ is the Hamiltonian, $\mathbf{r}_i$ and $\theta_i$ denote the position and orientation of particle $i$, $T$ is the temperature. For periodic lattices the orientational degrees of freedom $\theta_i$ of different particles can be decoupled and integrated out (Methods) with assumptions met by the very physical system we seek to explain, colloids in liquid suspension[5]: the Hamiltonian includes only interactions between nearest neighbours owing to their short-range nature. It is reasonable to consider only small fluctuations around the equilibrium configuration, as nearest-neighbour bonds are sufficiently permanent owing to the high energetic penalty of breaking a bond (approximately $7k_\mathrm{B}T$; ref. 21), and rotational fluctuations—as well as the number of orientational microstates—are limited by patch size[7,22] as attraction is approximately constant within the patch and dies off sharply at the patch boundaries. After the integration step we arrive at an effective Hamiltonian that depends on particle positions only, with the particle orientational degrees of freedom contributing an entropic term that poses preferences on bond angles. Figure 2a,b shows the dependence of rotational entropy on bond-angle differences. Clearly, rotational entropy is maximum when bond angles are equal.

These periodic arrangements are thus mechanically stable because energy constrains fluctuations of bond length and rotational entropy constrains fluctuations of bond angle. As anharmonicity does not qualitatively change the conclusions and can be regarded as renormalization of the mode structure (see below), for transparency we adopt the harmonic approximation and investigate the mode structure analytically using lattice dynamics[23]. The dynamical matrix $D$ of the lattice then has two parameters, a spring constant $k$ describing the central-force potential between nearest neighbours, and a bond-bending rigidity $\kappa = (3/2)k_\mathrm{B}T/(\phi - \pi/6)^2$ that results from approximating the rotational entropy by a quadratic form, where $\phi$ is the half-opening angle of the attractive patch defined in Fig. 2 ($\kappa$ is derived in Methods).

[1]Department of Physics and Astronomy, University of Pennsylvania, Philadelphia, Philadelphia 19104, USA, [2]Department of Physics, University of Michigan, Ann Arbor, Michigan 48109, USA, [3]Department of Materials Science and Engineering, University of Illinois, Urbana, Illinois 61801, USA, [4]Department of Chemistry, University of Illinois, Urbana, Illinois 61801, USA, [5]Department of Physics, University of Illinois, Urbana, Illinois 61801, USA.
*e-mail: maox@umich.edu.

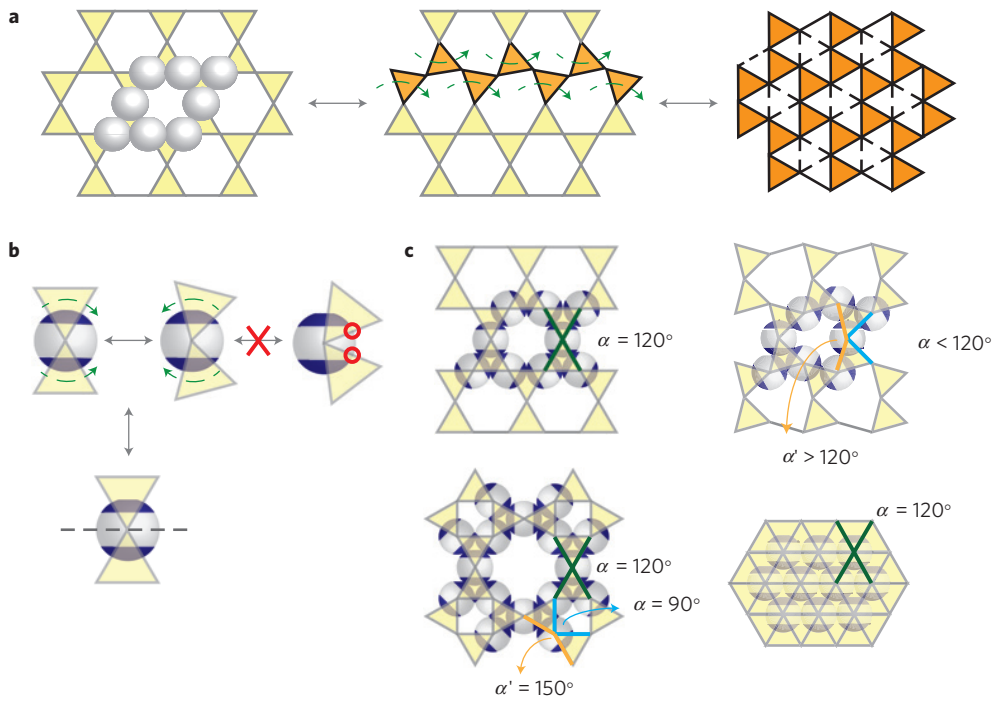


**Figure 1 | Examples of 2D open lattices. a**, Spheres with isotropic, central-force nearest-neighbour interactions in a hypothetical kagome lattice exhibit floppy modes (green arrows in middle image) rendering the lattice unstable to collapse into a close-packed structure (right image). **b**, Bond-angle changes of triblock Janus particles produce states of equal potential energy if particles have four contacts in the attractive patches (blue), and produce increased potential energy if the bond-angle change goes beyond the attractive patch (top right). Grey dashed lines represent possible additional contacts in the non-attractive middle band of the particle, as observed for close-packed cases. **c**, Examples of isoenergetic lattices formed by triblock Janus particles: in clockwise order, kagome, twisted kagome, hexagonal and Roman mosaic. Bond angles are shown in the figure.

More specifically, the effective Hamiltonian is

$$H_{\text{effective}} = \frac{k}{2}\sum_{(i,j)}(|\mathbf{r}_j - \mathbf{r}_i| - l)^2 + \frac{\kappa}{2}\sum_i(\Delta\alpha_i)^2 \qquad (2)$$

$$= \frac{1}{2}\sum_{l,l'}\vec{U}_l D_{l,l'}\vec{U}_{l'} \qquad (3)$$

where $\Delta\alpha_i$ describes the bond-angle difference of particle $i$ as defined in Fig. 2, $D$ is the dynamical matrix, and $l$ labels the unit cells. The first term in equation (2) corresponds to central-force potential and the second is the contribution from the rotational entropy. A two-dimensional (2D) kagome lattice has three particles in each unit cell, so $U_l$ is a six-dimensional vector denoting vibrations of the three particles. The mode structure, representing the square root of the eigenvalues of $D$ in momentum space, is shown in Fig. 2c. Without rotational entropy ($\kappa = 0$) a branch of phonon modes with zero frequency sits between the Γ and M points in the first Brillouin zone; interpreted physically, they are the floppy modes of the central-force-only kagome lattice illustrated in Fig. 1. But for patchy colloidal systems wherein $\kappa > 0$, these floppy modes are lifted to finite frequency, making the lattice mechanically stable. The lifted floppy modes hybridize with the transverse phonons, and thus the lowest branch of modes in the $\kappa > 0$ mode structure in Fig. 2c is a linear combination of the floppy mode and the transverse phonon[14]. This is the prediction.

In experiments, we calculated the correlation functions by tracking thermal vibrations of the particles of the kagome lattice. These correlation functions are related to the dynamical matrix by $\langle U_l U_{l'}\rangle = k_B T D^{-1}_{l,l'}$. This gives $k$ and $\kappa$ by fitting to the experimental data using this equation in momentum space[24,25]. Our experiments presently have a positional resolution of 0.05 μm, signifying that in a mode-structure plot we can resolve only data below 20 $\mu m^{-1}$. For comparison to theory, this led us to choose the lowest branch of modes between the points denoted Γ and M to fit our parameters, obtaining $k = (2{,}300 \pm 800)k_B T a^{-2}$ and $\kappa = (33 \pm 7)k_B T$, where $a = 2$ μm is the particle diameter.

As a technical note, this $k$ value describes the renormalized spring constant corresponding to large fluctuations (low frequency). Given the nature of hydrophobic attractions, renormalized values at higher frequencies are expected to be smaller. The $\kappa$ value does not have a strong frequency dependence, and corresponds to an effective patch size $\phi_{\text{exp}} = ((\pi/6) + 0.21 \pm 0.02) \cong (42 \pm 1)°$. This makes physical sense, as it is larger than $\pi/6$, the geometrical lower limit of the patch size, and smaller than 65°, the patch size measured by scanning electron microscopy (SEM). The quantitative difference from the SEM measurement may reflect roughness in experimental patch boundaries. The agreement on the mode structure between theory and experiment can be considered to be good.

This resolves the puzzle with which this paper began, that is, why the kagome lattice is stable mechanically for bond-angle changes, rotational entropy of patchy particles leads to an increase of the effective Hamiltonian even though the potential energy is flat. The kagome lattice gains constraints pertinent to the stability argument of Maxwell. Lattices whose bond angles differ from the optimal kagome lattice (Fig. 1c) have even higher free energy. However, further analysis is needed to explain the selection of the kagome over the hexagonal lattice, both of which possess the same optimal bond angle and thus the same rotational entropy per particle. The answer lies in the vibrational entropy.

The elastic free energy per particle $f$ is

$$f = -\frac{k_B T}{N}\ln Z = \frac{k_B T}{2N}\ln Det\, D + c \qquad (4)$$

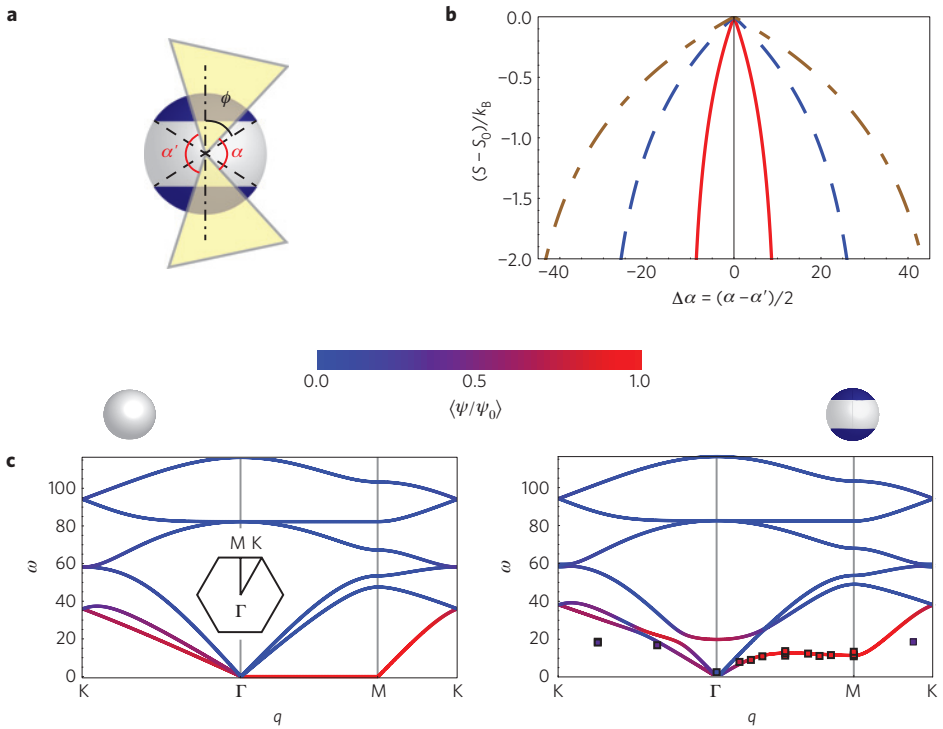


**Figure 2 | Predicted entropy in 2D open colloidal structures and comparison with experiment. a**, Definition of parameters: half-opening angle $\phi$ of attractive patches, and bond angles $\alpha$ and $\alpha'$. Triangles denote bonds with neighbours. Black dashed lines point to the boundaries of the attractive patches. The black dash-dotted line joins the north and south poles of the sphere. **b**, How the relative rotational entropy of a particle depends on bond-angle differences for three patch sizes, $\phi = 55°$ (brown), 45° (blue) and 35° (red). Here, $S$ and $S_0$ are the rotational entropies for $\Delta\alpha = (\alpha - \alpha')/2$ and $\Delta\alpha = 0$, respectively. **c**, Mode structures of the kagome lattice from isotropic particles (left) and triblock particles with angle-bending rigidity (right). Curves show the mode frequency in the harmonic approximation, obtained by fitting the lowest branch to experimental data (squares), as other branches have frequencies beyond the experimental precision. The colour scale, blue to red, represents the increasing overlap of the corresponding eigenmode $\psi$ with the floppy modes $\psi_0$ depicted in Fig. 1. Frequency $\omega$ is normalized by $\sqrt{k_B T/m}$, where $m$ is the particle mass, and plotted in units of $a^{-1}$.

where $N$ is the total number of particles and $c$ is a constant (Methods). The more the particles are confined by the lattice structure, the less the vibrational entropy, hence the higher the elastic free energy per particle. Illustrating this, Fig. 3a shows that in a close-packed hexagonal lattice each particle has, in addition to the same interactions as those in the kagome lattice, two central force contacts at middle bands with strongly screened electrostatic repulsion. Harmonic potentials with spring constant $k_r$ quantify this interaction expanded around the equilibrium configuration. This is why a close-packed lattice possesses higher free energy than the kagome lattice despite having the same rotational entropy per particle. The quantitative comparison is shown in Fig. 3b.

This entropic selection of open lattices over closely packed ones remains correct when the anharmonicity of the interactions is considered. Different polymorphs of the same type of particle share the same anharmonic interaction, the difference being that a particle in the hexagonal lattice possesses two additional central force bonds. This leads to stronger confinement for any anharmonicity, hence higher free energy. Moreover, the free-energy expression (equation (4)) is dominated by low-frequency terms for which the harmonic interaction is a good approximation.

The mathematical preference for the kagome lattice is significant enough to matter physically. The relative free energy of the alternative lattices depends on dimensionless ratios: $\kappa/(ka^2)$ and $k_r/k$. Figure 3b shows differences between the free energy per particle as a function of $\kappa/(ka^2)$ at three different values of $k_r/k$; preference for the kagome lattice decreases as $\kappa/(ka^2)$ increases. Using a free-energy difference of $k_B T$ per particle as the criterion of when it is significant enough to matter, we conclude that the kagome lattice is preferred roughly when $\kappa/(ka^2) < 1$, for $k_r$ within a reasonable range $(1 < k_r/k < 50)$, leading to a critical patch angle $\phi_c \sim \pi/6 + \sqrt{3k_B T/2\kappa a^2} \approx 31.5°$. This predicts that the wider the attractive patches on particles, or the stronger the central-force interactions, the more favoured is their assembly into a kagome lattice, even though they exhibit lower rigidity against change of bond angle if the patch is too wide.

To calculate the phase diagram, we alter the statistical mechanical ensemble appropriately and arrive at Fig. 3d. The horizontal axis is pressure normalized by both temperature and unit cell area because the aim is to compare the effects of entropy and pressure. Equivalently, by increasing pressure, and/or by decreasing temperature, the kagome lattice transforms to a close-packed one. It is noteworthy that the phase boundary, determined by equalizing the Gibbs free energy for the two lattices, has a non-zero intercept on the pressure axis. Below this pressure the kagome lattice is more stable, regardless of patch angle $\phi$. The positive slope of the transition line is because greater $\phi$ engenders smaller $\kappa/(ka^2)$, thus stronger entropic stabilization.

Experimentally, this was tested by raising the lateral pressure on the system. In an earlier experiment from this laboratory[5] it was not possible to do so as the kagome lattice was formed from latex spheres residing in an open chamber without a way to pressurize it. We here redesigned the experiment by employing denser (silica) particles and the triblock character was produced using a newly-developed method[6]. These spheres, placed in a tilt chamber, tend to sediment and we confirmed the close-packed-lattice phase under pressure (Fig. 3c). In fact, the lateral pressure increases along the projection of gravity in the tilted plane $x$. We observe the close-packed lattice only for $x > x_c$, indicating a critical pressure $p_c \approx 7k_B T/a^2$ above which it is stable. In Fig. 3d,

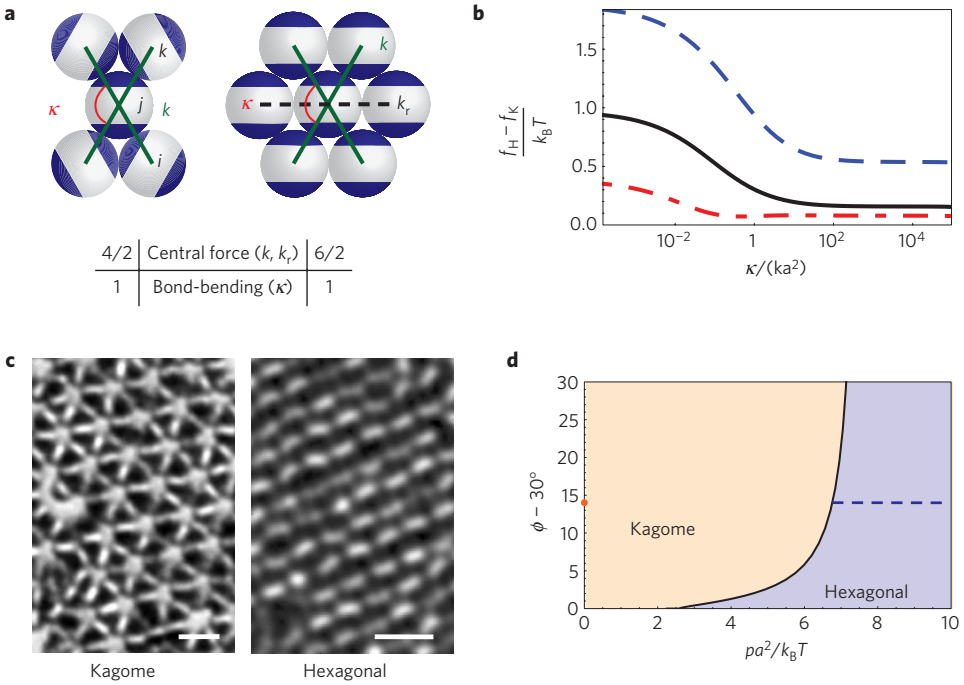


**Figure 3 | Predicted phase diagram and comparison with experiment. a**, Depiction of kagome and close-packed lattices in the harmonic lattice-dynamics model. Each particle in a kagome lattice experiences two attractive 'bonds' (central-force potentials) and one effective bond-bending potential arising from entropic fluctuations. Each particle in a close-packed lattice experiences an additional central-force potential of spring constant $k_r$ in its middle band. **b**, Free-energy-per-particle difference between these lattices as a function of the ratio $\kappa/ka^2$. The curves, from bottom to top, correspond to $k_r/k = 0.1, 1, 10$. **c**, Experimental bright-field optical-microscope images of kagome (left) and close-packed lattices (right) formed from silica spheres. Black regions are hydrophobic patches. Scale bars, 4 μm. **d**, Comparison between the theoretical phase diagram (phase boundary shown as a line) calculated using experimentally deduced values ($k = 2{,}300 k_B T\, a^{-2}$ and $k_r/k = 20$) and experimental data using silica particles with a patch size $\phi \approx 42°$. Orange dot: experimental kagome lattice at $p = 0$. Blue line: experimental hexagonal lattices at various lateral pressures. Although not considered here, on physical grounds one also expects melting at a sufficiently high temperature.

we show this experimental result as a line and compare it with the theoretical prediction. The value of $k_r/k \sim 20$ used in plotting the theoretical phase diagram was determined by comparing these new experiments to the theory.

An instructive thermodynamic argument explains qualitatively how relative stability depends on patch size. At finite pressure, the preference for the kagome lattice can be expressed in the form of a Gibbs free energy per particle $\Delta G = G_{HEX} - G_{Kagome} = \Delta E - T\Delta S + p\Delta V$, where $\Delta E = 0$ because the lattices are isoenergetic. Therefore, the phase boundary at $\Delta G = 0$ is simply $p = (\Delta S/\Delta V)T$, which is linear in the $p$–$T$ plane. The volume difference $\Delta V$ is constant (ignoring the small changes of volume for the given lattices as pressure changes), so the slope of the $p$–$T$ phase boundary is controlled by $\Delta S$. Physically, patch size influences $\Delta S$ through its effect on the allowed thermal fluctuations of the lattices. From this perspective, it makes sense that particles with larger patches have a more flexible structure. Possessing more entropy, their slope in the $p$–$T$ phase boundary is steeper. A technical point is that patch sizes above 60° are not meaningful, as then the lattice structure would allow three neighbours of a given sphere in two dimensions and different configurations must be considered. The main point is that although linearity of the phase boundary agrees nicely with a recent simulation for the range of parameters that were simulated[7], the theory also captures the additional dependence on patch size. To see the latter in simulation would have required long and expensive calculations, but it emerges naturally from the theory.

The theory likewise provides guidance on how to produce open 3D lattices using patchy colloids. Using the same triblock colloids as the earlier example, various lattices are predicted depending on the patch size. For example, if each patch allows three contacts, $35.5° < \phi < 45°$, the structural motif is the corner-sharing tetrahedron shown in Fig. 4a,b. Then the pyrochlore lattice, which is isostatic under central forces, becomes a natural candidate for the self-assembled structure. The entropy arguments just presented suggest interesting predictions. First, we expect the interplay between vibrational entropy and pressure to lead to a the interplay between open pyrochlore and close-packed face-centred cubic (fcc) lattices[8] that follows a linear phase boundary in the $p$–$T$ phase diagram, like the transition between kagome and hexagonal lattices in 2D. Second, although torsion between two corner-sharing tetrahedra costs no potential energy, and this implies multiple iso-energetic polymorphs, calculation of 3D rotational entropy shows that staggered configurations enjoy the most rotational entropy (Fig. 4a). We predict that this entropic difference may encourage selection of the pyrochlore lattice for a predictable range of parameters. If each patch allows four contacts, $45° < \phi < 58.3°$, the repeat motif is a corner-sharing octahedron, and one expects a similar transition between the open perovskite structure (Fig. 4c) and fcc lattices. Indeed, observation of a monolayer perovskite from triblock particles has been reported from phenomenological observation[5], but without theoretical understanding.

To form the famous diamond lattice by self-assembly is another grand challenge of materials science, with numerous potential applications in photonics[26]. This lattice (Fig. 4d) has coordination number four, less than the central-force isostatic point in $d = 3$, and has been studied via simulation for colloidal particles with four attractive patches of tetrahedral symmetry[27] (Fig. 4d). It differs only in vibrational entropy from close-packed bcc lattices, analogous to the kagome and close-packed phases of triblock Janus particles discussed above. Our theory predicts the phase boundary to be linear

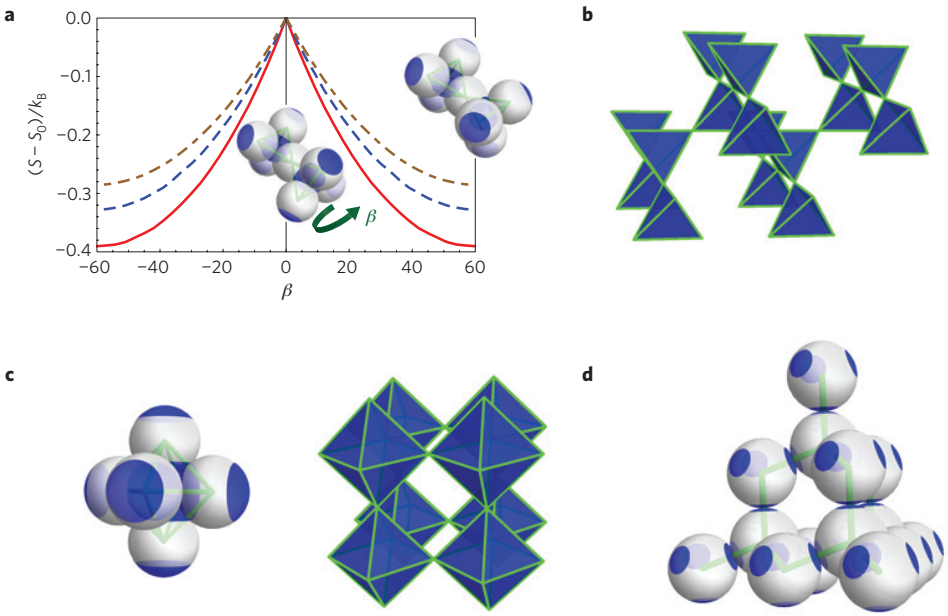


**Figure 4 | Predicted 3D structures. a**, Rotational entropy of a triblock particle at the pivot of two corner-sharing tetrahedra as a function of torsion angle $\beta$, for patch sizes $\phi = 36°$ (red), 40° (blue) and 44° (brown). **b**, Pyrochlore lattice as a candidate 3D structure of triblock particles with three contacts per patch. **c**, Perovskite lattice as a candidate 3D structure of triblock particles with four contacts per patch. The octahedron on the left, made up of six particles, is the structural unit. **d**, Diamond structure as a candidate 3D structure, consisting of 4-patch Janus particles. This lattice and close-packed body-centred cubic (bcc) lattices of the same particles differ in vibrational entropy, analogous to the kagome-hexagonal phases of triblock Janus particles in 2D cases.

in the $p$–$T$ plane, and the slope to increase as $\kappa/(ka^2)$ decreases. This agrees nicely with the numerical results in Fig. 2 of ref. 27, in which the phase boundary indeed is linear and for shorter interaction ranges (greater $k$ in the harmonic approximation) exhibits larger slope. Thus the theoretical framework developed here extends easily to 3D assembly, to cases where experimental efforts have long been held back by an insufficient understanding of which parameter spaces are most promising to implement in the laboratory.

## Methods

**Theory to decouple particle orientations.** In principle, the potential between two colloidal particles can be expressed as an integral over the surface area of the two particles. However, if the interactions between the two surfaces are sufficiently short-ranged, and the two particles are sufficiently close, the surface elements crossed by the line connecting their centres dominate the potential. Then the potential energy between the two particles can be written as

$$\mathcal{V}(\mathbf{r}_i,\theta_i,\mathbf{r}_j,\theta_j) \cong v(|\mathbf{r}_i-\mathbf{r}_j|)w(\hat{e}_{ij},\theta_i)w(\hat{e}_{ji},\theta_j)$$

where $\hat{e}_{ij}$ is the unit vector pointing from particle $i$ to $j$, and $w$ describes the property of the surface element crossed by $\hat{e}_{ij}$ given the particle orientation $\theta_i$. The Kern–Frenkel potential is an example of such a potential with the orientations of the two particles decoupled into two $w$ factors[22].

Here we are interested in small fluctuations around equilibrium periodic lattices. Thus if a contact is made in the attractive patches of two particles in the equilibrium configuration (we shall call this an 'attractive bond'), then in the partition function we only include configurations that keep this contact in the attractive patches because of the prohibitively large potential energy to break this bond. Therefore we model the orientational dependence for triblock particles

$$w(\hat{e}_{ij},\theta_i) \equiv \begin{cases} 1, & |\hat{e}_{ij}\cdot\hat{n}_i| \geq \cos\phi \\ \infty, & |\hat{e}_{ij}\cdot\hat{n}_i| < \cos\phi \end{cases}$$

where $\hat{n}_i$ is the unit vector pointing to the north pole of the particle. Thus the partition function of the whole system can be written as

$$Z = \int \mathrm{e}^{-H_{\mathrm{CF}}(\{\mathbf{r}_i\})/k_{\mathrm{B}}T} \prod_j \Psi_j(\{\mathbf{r}_i\},\theta_j)\,\mathrm{d}\mathbf{r}_j\,\mathrm{d}\theta_j$$

where $H_{\mathrm{CF}}$ is the central force part of the Hamiltonian, which depends only on the positions of the particles. The factors $\Psi_j(\{\mathbf{r}_i\},\theta_j) = 1$ when the attractive bonds of the $j$th particle remain in the attractive patch of $j$, and equal 0 otherwise, regardless of the orientations of other particles. The orientations of different particles are then decoupled and can be integrated out, contributing a rotational entropy term $s_j$ to the total effective Hamiltonian

$$H_{\mathrm{effective}} = H_{\mathrm{CF}} - T\sum_j s_j$$

$$s_j = k_{\mathrm{B}}\ln\int \Psi_j(\{\mathbf{r}_i\},\theta_j)\mathrm{d}\theta_j$$

**Rotational entropy of triblock particles.** Confining the rotation of triblock particles to the plane, which describes the experiments in this paper, the rotational entropy is

$$s_j = k_{\mathrm{B}}\ln[2(\phi-\frac{\pi}{6})-|\Delta\alpha_j|]$$

The result is plotted in Fig. 2, along with the definitions of $\phi$ and $\Delta\alpha_f$. To obtain this simple form we assumed that the angles between upper and lower bond pairs of a particle remain 60° because bond-length fluctuations are less than those of the 120° angle (which are the floppy modes and thus exhibit large fluctuations, as can be seen from the experimental data in Fig. 2c). In actual calculation of free energy we include the small corrections for these fluctuations, but this changes nothing qualitatively.

We also studied the case in which particles are allowed to rotate in 3D space, the lattice still kept as a 2D monolayer. Although Supplementary Information shows that the results are mathematically more complex, the resulting rotational entropy depends on the patch size and bond angles in a fashion similar to the 2D case.

Furthermore, to characterize harmonic lattice dynamics, we approximate the rotational entropy $s_j$ as a quadratic potential with equivalent second moment of fluctuations

$$s_j \approx -\frac{3k_{\mathrm{B}}}{4(\phi-\frac{\pi}{6})^2}(\Delta\alpha_j)^2$$

from which we define the bond-bending rigidity $\kappa$.

**Comparison of experiment to theory.** Triblock latex particles were produced and allowed to self-assemble using an experimental protocol and experimental conditions the same as described previously[5], except that, to produce higher effective pressures, it was necessary to use silica colloids[6] and a newly designed tilt cell. Phonon spectra of the kagome lattice were calculated from image analysis, as described in the text. The images have a positional resolution of 0.05 μm.

**Calculation of free energy and phase boundary.** Using equations (2) and (4), free energies of the kagome and the hexagonal lattices can be calculated. For the two lattices considered here, Fig. 3a shows the relevant interactions of each particle involved. A detailed construction of the dynamical matrix for a kagome lattice has been shown in ref. 28, and for this problem one simply needs to add in bond-angle terms in which we express the bond angle change as

$$\Delta\alpha = \frac{1}{\alpha}[\hat{e}_{jk} \times (\vec{u}_k - \vec{u}_j) - \hat{e}_{ij} \times (\vec{u}_j - \vec{u}_i)]$$

where $i, j, k$ are the three particles that form the 120° angle as labelled in Fig. 3a. Because the free energy depends on the logarithm of the dynamical matrix, one can factorize out the central force spring constant, which then becomes an additive constant, and thus it follows that the free energy difference between polymorphs of the same type of particles depends only on the ratios of the spring constants. The free energy difference can then be calculated as an integral in the first Brillouin zone numerically (we add in small corrections from the fluctuation of those 60° bond angles in the actual calculation), with the result shown in Fig. 3b. The calculation of the phase boundary follows the equal Gibbs free energy line of the two lattices, as we discussed, $P = \Delta F / \Delta V$.

Received 17 May 2012; accepted 22 October 2012; published online 13 January 2013

## References


1. Antlanger, M., Doppelbauer, G. & Kahl, G. On the stability of Archimedean tilings formed by patchy particles. *J. Phys. Condens. Matter* **23,** 404206 (2011).
2. Torquato, S. Inverse optimization techniques for targeted self-assembly. *Soft Matter* **5,** 1157–1173 (2009).
3. Cohn, H. & Kumar, A. Algorithmic design of self-assembling structures. *Proc. Natl Acad. Sci. USA* **106,** 9570–9575 (2009).
4. Edlund, E., Lindgren, O. & Jacobi, M. N. Novel self-assembled morphologies from isotropic interactions. *Phys. Rev. Lett.* **107,** 085501 (2011).
5. Chen, Q., Bae, S. & Granick, S. Directed self-assembly of a colloidal kagome lattice. *Nature* **469,** 381–384 (2011).
6. Chen, Q. *et al.* Triblock colloids for directed self-assembly. *J. Am. Chem. Soc.* **133,** 7725–7727 (2011).
7. Romano, F. & Sciortino, F. Two-dimensional assembly of triblock Janus particles into crystal phases in the two bond per patch limit. *Soft Matter* **7,** 5799–5804 (2011).
8. Romano, F. & Sciortino, F. Patterning symmetry in the rational design of colloidal crystals. *Nature Commun.* **3,** 975 (2012).
9. Khalil, K. S. *et al.* Binary colloidal structures assembled through Ising interactions. *Nature Commun.* **3,** 794 (2012).
10. Glotzer, S. C. & Solomon, M. J. Anisotropy of building blocks and their assembly into complex structures. *Nature Mater.* **6,** 557–562 (2007).
11. Galisteo-López, J. F. *et al.* Self-assembled photonic structures. *Adv. Mater.* **23,** 30–69 (2011).
12. Su, B-L., Sanchez, C. & Yang, X-Y. *Hierarchically Structured Porous Materials: From Nanoscience to Catalysis, Separation, Optics, Energy, and Life Science* 55–129 (Wiley, 2012).
13. Maxwell, J. C. On the calculation of the equilibrium and stiffness of frames. *Phil. Mag.* **27,** 294 (1864).
14. Souslov, A., Liu, A. J. & Lubensky, T. C. Elasticity and response in nearly isostatic periodic lattices. *Phys. Rev. Lett.* **103,** 205503 (2009).
15. Kapko, V., Treacy, M., Thorpe, M. & Guest, S. On the collapse of locally isostatic networks. *Proc. R. Soc. Lond. A* **465,** 3517 (2009).
16. Hammonds, K. D., Dove, M. T., Giddy, A. P., Heine, V. & Winkler, B. Rigid-unit phonon modes and structural phase transitions in framework silicates. *Am. Mineral.* **81,** 1057–1079 (1996).
17. Sun, K., Souslov, A., Mao, X. & Lubensky, T. C. Surface phonons, elastic response, and conformational invariance in twisted kagome lattice. *Proc. Natl Acad. Sci. USA* **31,** 12369–12374 (2012).
18. Guest, S. D. & Hutchinson, J. W. On the determinacy of repetitive structures. *J. Mech. Phys. Solids* **51,** 383–391 (2003).
19. Yodh, A. *et al.* Entropically driven self-assembly and interaction in suspension. *Phils. Trans. R. Soc. Lond. A* **359,** 921–937 (2001).
20. Meng, G. *et al.* The free-energy landscape of clusters of attractive hard spheres. *Science* **327,** 560–563 (2010).
21. Chen, Q. *et al.* Supracolloidal reaction kinetics of Janus spheres. *Science* **331,** 199–202 (2011).
22. Kern, N. & Frenkel, D. Fluid–fluid coexistence in colloidal systems with short-ranged strongly directional attraction. *J. Chem. Phys.* **118,** 9882–9889 (2003).
23. Born, M. & Huang, K. *Dynamic Theory of Crystal Lattices* (Clarendon, 1998).
24. Keim, P., Maret, G., Herz, U. & von Grünberg, H. H. Harmonic lattice behavior of two-dimensional colloidal crystals. *Phys. Rev. Lett.* **92,** 215504 (2004).
25. Ghosh, A. *et al.* Density of states of colloidal glasses. *Phys. Rev. Lett.* **104,** 248305 (2010).
26. Ho, K. M., Chan, C. T. & Soukoulis, C. M. Existence of a photonic band gap in periodic dielectric structures. *Phys. Rev. Lett.* **65,** 3152–3155 (1990).
27. Romano, F., Sanz, E. & Sciortino, F. Role of the range in the fluid-crystal coexistence for a patchy particle model. *J. Phys. Chem. B* **113,** 15133 (2009).
28. Mao, X. & Lubensky, T. C. Coherent potential approximation of random nearly isostatic kagome lattice. *Phys. Rev. E* **83,** 011111 (2011).


## Acknowledgements

X.M. was supported by NSF under grant DMR-1104707. Q.C. and S.G. were supported by the US Department of Energy Division of Materials Science, under award number DE-FG02-07ER46471 through the Frederick Seitz Materials Research Laboratory at the University of Illinois at Urbana-Champaign. For equipment, we acknowledge the National Science Foundation, CBET-0853737. We thank K. Chen for help with particle tracking, and J. Whitmer and T. C. Lubensky for useful discussions.

## Author contributions

X.M. and Q.C. initiated this work; X.M. developed the theory and did calculations based on the theory; Q.C. and S.G. designed and performed the experiment; X.M., Q.C. and S.G. wrote the paper.

## Additional information

Supplementary information is available in the online version of the paper. Reprints and permissions information is available online at www.nature.com/reprints. Correspondence and requests for materials should be addressed to X.M.

## Competing financial interests

The authors declare no competing financial interests.